Engineering Geology 228 (2017) 82–96

Contents lists available at ScienceDirect

Engineering Geology

journal homepage: www.elsevier.com/locate/enggeo

Stability analysis of slide-toe-toppling failure

Mehdi Amini*, Akbar Ardestani, Mohammad H. Khosravi

School of Mining Engineering, College of Engineering, University of Tehran, Tehran, Iran

ARTICLE INFO

Keywords:
Rock slope
Secondary toppling failure
Slide-toe-toppling
Physical modeling
Theoretical approach

ABSTRACT

Toppling failure is a common mode of instability in layered and blocky rock slopes where rock blocks rotate about their toes and overturn. One of the most important types of toppling failure is slide-toe-toppling. In this failure, rock blocks at the toe of the slope are overturned by the pressure of sliding mass from the upper part of the slope. In the present study, this type of failure is examined through physical and theoretical modeling. The literature on toppling failures is reviewed briefly first and, then, the mechanism of slide-toe-toppling failure is described. To clarify the mechanism of the failure, a series of physical model tests is conducted under static condition by means of a new tilting table apparatus. Then, a theoretical approach is proposed based on limit equilibrium analysis and some new equations are developed for stability analysis of this type of failure. Finally, the results of physical modeling are compared with outcomes of proposed theoretical approach. This comparison shows a good agreement between the theoretical and experimental results.

1. Introduction

Toppling failure is a common instability in natural and excavated rock slopes. From the mechanism point of view, the toppling failures are classified as main and secondary (Goodman and Bray, 1976). In the main types of toppling failure (flexural, blocky and block-flexure), the primary cause of instability is weight of the rock mass. But, in the secondary types of toppling failure, rock mass is stimulated by some external factors. These types of failure are briefly described here. To understand the mechanism of blocky toppling failure, it is assumed that rock mass is composed of a set of dominant parallel discontinuities dipping steeply into the slope face and a set of cross-joints extended normal to the dominant discontinuities dividing the rock columns into a set of rock blocks. Under such condition, the rock blocks may slide along or turn over the natural cross-joins in their base; so their tensile strength has no significant effect on the stability of rock slope. Fig. 1-a shows a schematic diagram and a real case study of this instability. Another type of main toppling failure is flexural toppling. To understand the mechanism of this type of failure, it is assumed that a rock mass is only composed of a set of parallel persistent discontinuities dipping steeply into the slope face. As such, the rock mass behaves like a series of superimposed inclined continuous cantilever rock columns which are subjected to bending stresses. When bending tensile stress in the rock columns exceeds their tensile strength, they fail and topple downward. Fig. 1-b shows a schematic diagram of this instability and a photograph of such failure in a limestone quarry mine. In real case studies, the above-mentioned idealized failure mechanisms are not common. Natural toppling failures are mostly a combination of both blocky and flexural modes which can be generally termed as block-flexure toppling failure. If any of these failures is stimulated by some external factors, the result will be called a secondary toppling failure. Secondary toppling failures are quite diverse and many modes have been proposed for these failures. In Fig. 2, rock blocks at the toe of the slope are overturned by the pressure of sliding mass from the upper portion of the slope. This phenomenon is a combined failure known as slide-toe-toppling. In this paper, the mechanism of this failure is clarified through a series of physical model studies and a new flexible analytical approach is proposed.

2. Literature review

Failure due to overturning of natural rock blocks was first mentioned by Müller in 1968, after studying the instabilities near the Vaiont dam lake in Italy (Müller, 1968). In 1971, Ashby introduced a simple criterion for this type of failure and proposed the term “toppling” for it. From 1971 to 1976, toppling failure was the subject of a few scattered researches focused on numerical and physical modeling and real case studies (Cundall, 1971; De Freitas and Watters, 1973).

In 1976, Goodman and Bray classified the toppling failures into two categories: main (flexural, blocky and block-flexure) and secondary types and introduced a theoretical approach for the analysis of blocky mode. Later, several researchers tried to develop this approach into some design charts and computer programs to assess the failure (Hoek and Bray, 1977; Zanbak, 1984; Choquet and Tanon, 1985; Tatone and

* Corresponding author at: School of Mining Engineering, College of Engineering, University of Tehran, Northern Kargar Street, Tehran, Iran.
E-mail addresses: mamini@ut.ac.ir (M. Amini), akbarardestani@ut.ac.ir (A. Ardestani), mh.khosravi@ut.ac.ir (M.H. Khosravi).

http://dx.doi.org/10.1016/j.enggeo.2017.07.008
Received 4 April 2017; Received in revised form 22 June 2017; Accepted 17 July 2017
Available online 26 July 2017
0013-7952/

List of symbols

σ_t	Tensile strength of rock blocks
UCS	Uniaxial compressive strength
γ	Unit weight
h	Average length of blocks or slices
z	Height of falling
t	Thickness of blocks
ψ_f	Dip of slope face
ψ_p	Dip of dominant discontinuities of rock mass or soil slices
ψ_t	Dip of overall failure plane of toppling failure
ψ_s	Dip of upper surface of the slope
ψ_b	Dip of normal to discontinuities
b	Distance between tensile crack and crown of slope
n	Number of rock block
m	Number of soil slice
H	Height of slope
f_R^j	Inter-slice normal force acting at the right side of slice "j"
f_L^j	Inter-slice normal force acting at the left side of slice "j"
N^j	Normal force acting at the base of slice "j"
S^j	Shear force acting at the base of slice "j"
ψ_R^j	Angle between f_R^j and normal to slice "j"
ψ_L^j	Angle between f_L^j and normal to slice "j"
h_R^j	Point of application of f_R^j with respect to base of slice "j"
h_L^j	Point of application of f_L^j with respect to base of slice "j"
ℓ^j	Point of application of N^j with respect to toe of slice "j"
ψ_a^j	Dip of base of slice "j" with respect to horizon
Δx^j	Thickness of slice "j"
ϕ_s	Internal friction angle of soil
c_s	Cohesive strength of soil
ϕ_{sb}	Interface friction angle between soil and rock masses
ϕ_b	Interface friction angle of base of rock blocks
c_b	Cohesive strength of base of rock blocks
ϕ_c	Interface friction angle between adjacent rock blocks
ϕ_i	Internal friction angle of intact rock
c_i	Cohesive strength of intact rock
κ	Constant coefficient
W	Weight of rock blocks
P	Inter-block normal force
Q	Inter-block shear force
y	Point of application of "P" with respect to base of block

Grasselli, 2010). Apart from the above mentioned researches, many other articles and reports can be found in the literature on the physical modeling, case study and theoretical and numerical analysis of blocky toppling failure, mostly based on the classification of Goodman and Bray (Wyllie and Mah, 2004; Pritchard and Savigny, 1990; Bobet, 1999; Sagaseta et al., 2001; Naresh et al., 2002; Xinbin et al., 2007; Brideau and Stead, 2010; Alejano et al., 2015; Smith, 2015).

The first comprehensive approach to analyze flexural toppling failure was introduced by Aydan and Kawamoto (1992) who managed to incorporate the effects of dynamic loads and underground water pressure into the analysis. In 2009, Amini et al. proposed a simple and direct method for analysis of the failure based on compatibility principles governing the behavior of cantilever beams (Amini et al., 2009). There was a good agreement between the results of this method and the results of existing physical modeling and case studies. Apart from these studies, this type of failure has been the subject of several articles in the

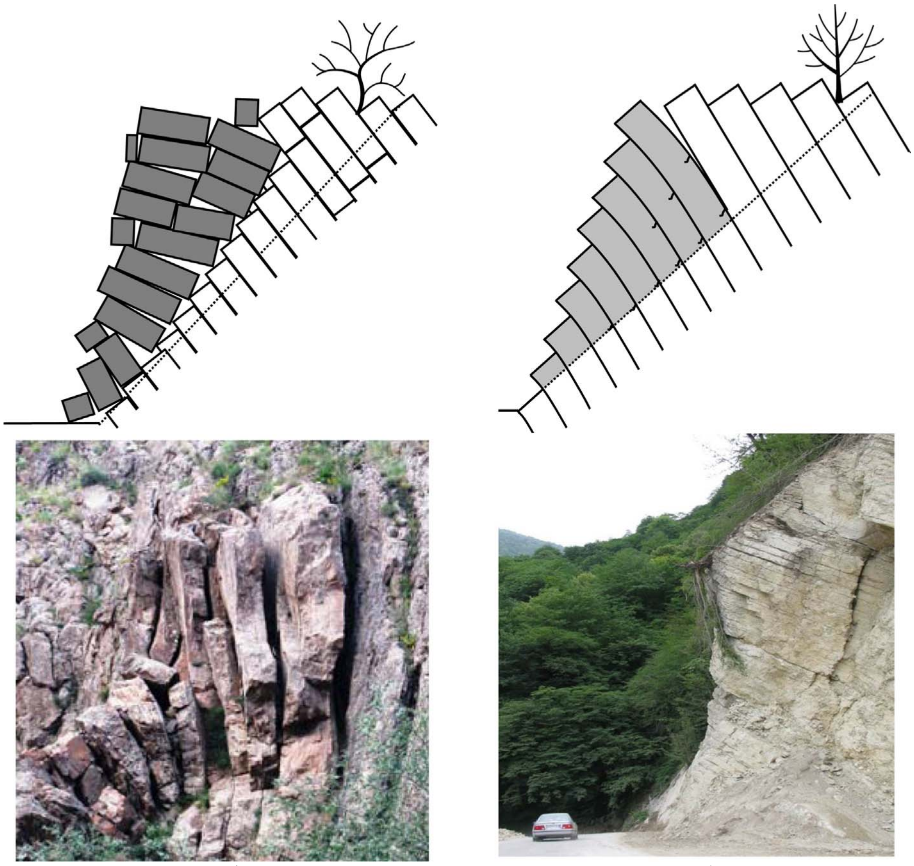

a) b)

Fig. 1. Schematic diagrams and real case studies of main toppling failures: a) blocky; b) flexural.

format of physical and numerical modeling and real case studies (Adhikary et al., 1997; Adhikary and Guo, 2002; Alzo'ubi et al., 2010; Aydan and Amini, 2009; Majdi and Amini, 2010).

In 2012 and 2015, Amini et al. combined the method of Goodman and Bray (1976) with the method of Aydan and Kawamoto (1992) to introduce a solution for analysis of block-flexure toppling failure. They evaluated their method on a number of case studies and demonstrated the validity and accuracy of its results. In 1983, Teme and West studied a particular case of slide-toe-toppling failure by basing their analysis on the assumption that sliding of a massive rigid block at the top leads to a blocky toppling failure at the toe of the slope (Teme and West, 1983). A typical example of this type of failure, occurred in the slopes of a coal open pit mine, was studied by Wyllie and Munn in 1979. In 2014, Amini proposed a new mechanism for this failure based on the assumption that the interactions between soil mass and rock columns are similar to the interactions between soil and a rigid retaining wall (Amini, 2014). Later, this method was developed by Mohtarami et al. (2014) and its results were validated in a real case study. However, the method is limited to a logarithmic spiral failure surface in the upper soil mass and block-flexure toppling failure in toe of the slope and, also, the theoretical analysis is too complicated. It is, hence, of utmost importance to study the mechanism of the failure and to evaluate it rationally. Effort has been made to study it in this paper.

3. Mechanism of slide-toe-toppling failure

As mentioned, when a slope is made of an upper portion susceptible to sliding and a lower portion prone to toppling failure, the slope has a potential of slide-toe-toppling. Schematic diagram of this type of failure is shown in Fig. (2). In this type of failure, analysis of the rock mass positioned at the toe of the slope shows that this part should be stable against toppling failure by its own weight. Hence, this section acts like a rigid wall retaining the independently unstable soil mass. Therefore, there is a natural reaction between soil and rock masses.

In the simplest case, the first top rock block is subjected to its own weight and a force exerted by the upper soil mass. But in general, this block could also be subjected to some external forces such as dynamic loads, water pressures and loads of rock bolts. In any case, resultant of all of the mentioned forces may push the block to topple or slide. This block also will push and destabilize the next block and this domino effect will continue down to the last block at the toe of the slope. Finally, if the last rock block slides or topples, the entire slope will fail and a slide-toe-toppling failure will occur; but as long as the last rock block remains stable, the slope will be stable too. Hence, to evaluate the stability of the slope, the reaction force between upper soil mass and the first top rock block should be known. But, sliding soil mass is statically indeterminate. Therefore, it should first be solved with appropriate theoretical methods and, then, its reaction with the first block should be estimated. In next sections, the mechanism of this instability is clarified by physical modeling and a new theoretical model is proposed to determine the reaction between the upper soil mass and the lower rock mass in the slide-toe-toppling failure.

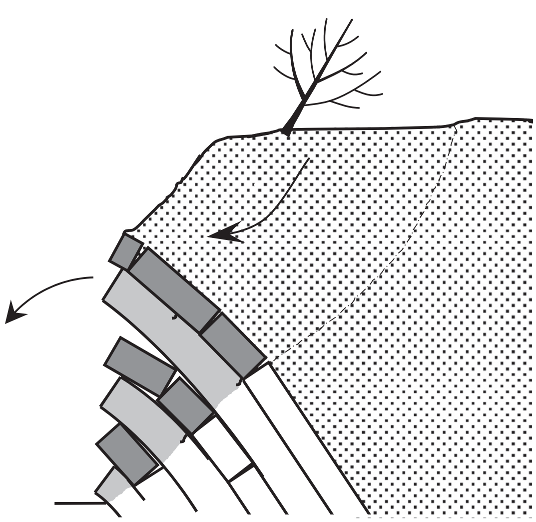

Fig. 2. Schematic diagram of slide-toe-toppling failure.

4. Modeling of slide-toe-toppling

4.1. Physical modeling

Physical modeling is a conventional method for studying the mechanisms of instabilities in soil and rock masses. These models play an essential role in validation of theoretical and numerical models and verification of their results. In the case of slopes, physical modeling is usually carried out by tilting table, centrifuge apparatus, base friction table and temporary support. In the tilting table method and temporary support, weight of samples is modeled directly; so the model should be large enough to naturally fail under its own weight. But in the centrifuge and base friction methods, weight is simulated with the aid of centrifugal and friction forces; so the model can be reasonably small (Khosravi et al., 2016). So far, the physical models developed for the study of toppling failures have been entirely focused on the main toppling failures (Ashby, 1971; Egger, 1983; Aydan and Kawamoto, 1992; Aydan and Amini, 2009; Amini et al., 2015) and no such model has developed for secondary toppling failures. In this study, the slide-toe-toppling failure was physically modeled to clarify the mechanism of this instability and check the validity of the outcomes of proposed theoretical approach. Details and results of this physical modeling are provided in the following subsections.

4.1.1. Material properties

The selection of modeling material is one of the most important issues in regard to physical modeling. In this study, all physical models were made with base friction powder. This powder is a frequently used material to construct physical models and is a highly regarded for this purpose (Egger, 1983; Kawamoto et al., 1983; Aydan and Kawamoto, 1992; Aydan and Amini, 2009, Amini et al., 2015). When the powder is poured in suitable molds and properly compressed, it turns into solid blocks of desired quality (Fig. 3). The higher is the pressure, the denser and thus stronger will be the resulting block. Thus, this powder can be used to prepare blocks of desired strength and unit weight in line with research purposes. The high unit weight and low strength of the resulting blocks make them particularly suitable for physical modeling on tilting table, as they allow the model to fail under its own weight even in a small scale. In the models of this study (for examination of slide-toe-toppling failure), this powder was used as a homogenous material constituting the upper portion of the slope and the solid blocks made of compressed powder were used to build the rock mass at the toe portion.

Fig. 3. Mold, powder and solid blocks used in this research.

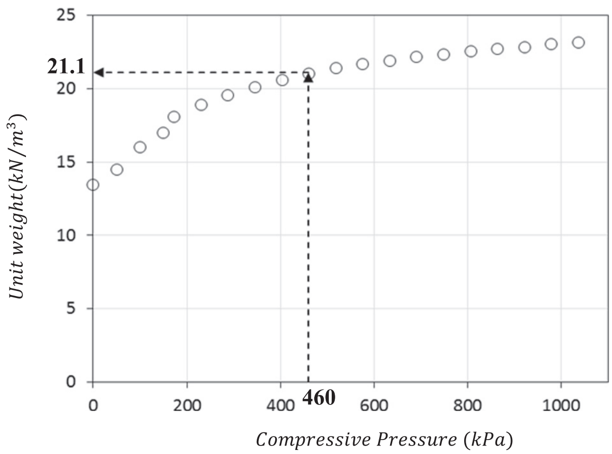

Fig. 4. Variation of blocks' unit weight versus compressive pressure.

Evaluation of physical models with numerical and theoretical methods requires an adequate measurement of mechanical and physical properties of the modeling material. Therefore, powder and solid blocks were subjected to a number of initial tests to determine the required properties.

4.1.1.1. Unit weight. The unit weight of a solid blocks could be controlled by the compressive pressure (0–1036 kPa) applied to the base friction powder. The resultant unit weight is plotted as a function of molding pressure in Fig. 4. As expected, the unit weight of the block increased with an increase in molding pressure. But this relationship was not linear; because the mold had a fixed initial volume and as the pressure increased and specimen became more compressed, compression progressed at a slower rate. In this study, the blocks were made under a pressure of 460 kPa, resulting in a unit weight of 21.1 kN/m^3 (Fig. 4).

To simulate the soil mass behind the rock blocks, the same base friction powder was used under its loose condition. The air pluviation technique was applied where the material is poured into the modeling box from a certain falling height. A feeder was produced for this purpose with the ability to move along the modeling box and with a controllable falling height. The powder was poured from different falling heights (5, 10, 15 and 20 cm) into a small box with known volume and a relationship between the falling height and resultant unit weight was defined (Fig. 5).

As it can be seen, in the scope of this study, powder's unit weight showed an almost linear relationship with the falling height which is expressed as the following equation:

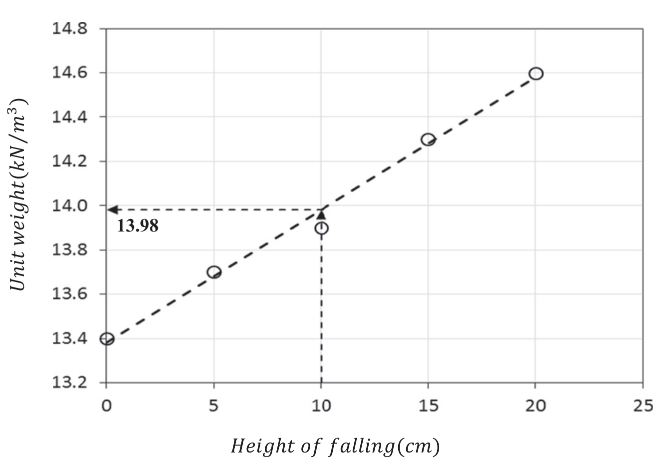

Fig. 5. Relationship of powder's unit weight with height of falling.

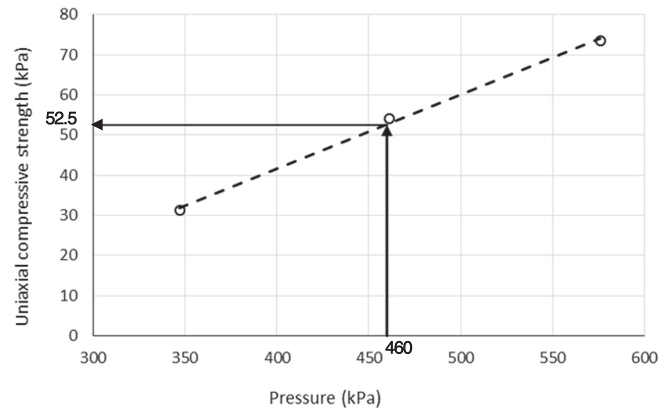

Fig. 6. Variation of the block's uniaxial compressive strength versus compressive pressure.

$$\gamma = 0.06z + 13.38 \tag{1}$$

where z is the falling height in cm and γ is the powder's resultant unit weight in kN/m^3. In this study, the soil mass in physical models was made with a falling height of 10 cm, resulting in a unit weight of 13.98 kN/m^3.

4.1.1.2. Uniaxial compressive strength. Uniaxial compressive strength of solid blocks is one of the most important mechanical properties of these material which acts as a measure of blocks' strength and competency and a criterion for the choice of ultimate compressive pressure. The blocks should be strong enough to sustain their shape during preparation in the model; but weak enough to fail under modeling stress level. To determine the relationship between blocks' compressive strength and molding compressive pressure, uniaxial compressive strength of several specimens made under pressures of 346–570 kPa was measured. All of these specimens were 5 cm wide, 10 cm high and had a thickness of between 3.7 and 3.9 cm depending on the molding compressive pressure. The trend of uniaxial compressive strength versus compression pressure (in the scope of this study) is plotted in Fig. 6. This figure shows that in the mentioned pressure range (346–570 kPa), the block's uniaxial compressive strength has a linear relationship with molding compressive pressure. Note that over a wider range, this relationship is likely to be nonlinear; but, when the compressive pressure ranges from 246 kPa to 570 kPa, the linear relationship is accurate enough to explain their association (see Fig. 4). Since the molding compressive pressure in this study was decided to be 460 kPa, the blocks' uniaxial compressive strength was assumed to be 52.5 kPa.

4.1.1.3. Tensile strength. As mentioned earlier, in flexural and block-flexure toppling failures, rock blocks first break under tensile stress and then overturn. Thus, these modes of failure are particularly sensitive to the blocks' tensile strength. This also applies to the case of physical models. In view of this sensitivity, tensile strength of solid blocks made under different compression pressures should be measured. Measuring the tensile strength of weak and brittle material is subject to many limitations. Hence, to measure this parameter, indirect test methods are more preferable. The common practice for determining the tensile strength of these blocks is the use of three-point or four-point bending tests. In these methods, especially in four-point bending test, stress concentration around supports may lead to crack initiation and propagation in those areas which results in a lower accuracy of the results. To avoid this issue, the authors designed and built a new device shown in Fig. 7 to measure the tensile strength in line with research objective. In this device, a 20 cm long block with a weight placed on its one end is placed on a small conveyor belt. As the motor starts, the belt starts to move and one end of the block start to hang off the edge and

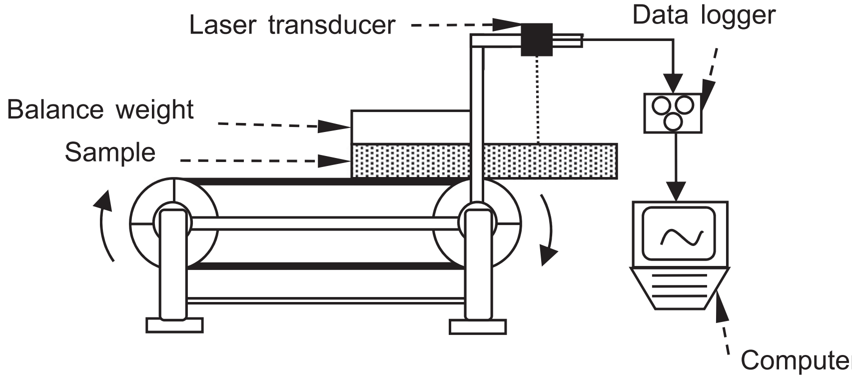

Fig. 7. Measurement of tensile strength of solid blocks by a new apparatus.

act as a cantilever beam. As the belt moves, the free length of this beam increases until the block breaks under its own weight. In this device, the moment of failure is determined by a laser displacement transducer installed above the hanging side of the specimen. According to the laws of solid mechanics, tensile strength of the block at the moment of failure can be determined by the following relationship:

$$\sigma_t = 3h^2\gamma/t \quad (2)$$

where h is the length of the block at the moment of failure, γ is the block's unit weight and t is the block's thickness.

In this study, several 5 cm thick blocks made under different compression pressures (346–570 kPa). Unit weight of these blocks was determined according to the diagram demonstrated in Fig. 4. For each block, its length at the moment of failure was measured by mentioned device and its tensile strength was obtained from Eq. (2). In Fig. 8, the block's tensile strength is plotted versus compression pressure (346–570 kPa). As this plot shows, along the mentioned pressure range, the block's tensile strength has a linear relationship with molding compressive pressure. Note that, as stated for the uniaxial compressive strength, this relationship would be probably nonlinear over a wider pressure range. Since the solid blocks to be used in physical modeling were made under pressure of 460 kPa, in theoretical analyses, tensile strength of the blocks was assumed to be 14 kPa.

4.1.1.4. Shear strength parameters. In slide-toe-toppling failure, soil mass must undergo shear sliding and rock blocks must slide on each other before toppling. Thus, the internal shear parameters of both powder and blocks and also the inter-block shear parameters are important for analysis. The internal shear parameters were measured by direct shear test using a 6 × 6 cm shear box. In this test, dry base friction powder was poured into the box and was sheared under normal effective stresses of 1.8, 4.4 and 6.2 kPa. These results showed that the used powder had a friction angle of 20° and a cohesive strength of 0.35 kPa.

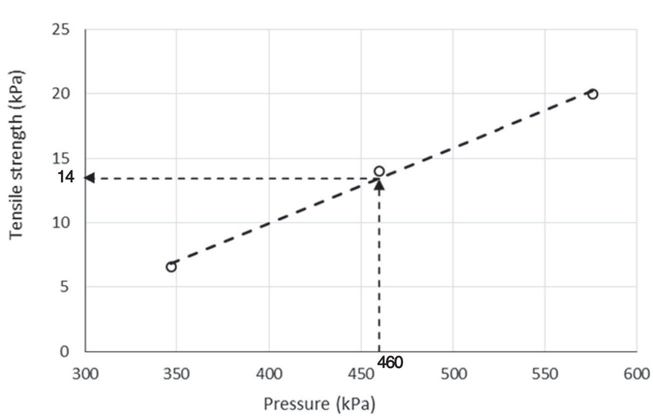

Fig. 8. Variation of the block's tensile strength versus compressive pressure.

To determine the internal shear strength parameters of the blocks, a number of blocks were made under pressure of 460 kPa and were tested as was described for powder (under normal effective stresses of 1.8, 4.4 and 6.2 kPa). The blocks exhibited a friction angle of 35° and a cohesive strength of 100 kPa. Also, the inter-block shear strength was estimated by some tests on a small tilting table. In these tests, one block was placed on top of another and the table was inclined until the top block slid. By ignoring the inter-block cohesive strength, the angle of the table at the onset of sliding will be equal to the inter-block friction angle. These tests showed that the inter-block friction angle is about 32°.

4.1.2. Physical model tests

Slide-toe-toppling failure was modeled on a tilting table designed and constructed at the University of Tehran by the authors specifically for this purpose. Fig. 9 shows a schematic diagram and a photograph of this apparatus. To use this device, physical model of the slope was built inside a 1 × 0.5 × 0.5 m transparent Plexiglas Acrylic box which was perfectly horizontal and fully fixed when building the model. Once the model was built, the box and hence the model were tilted very gently at a constant rate of 1° per minute. Angle of the tilting table was measured by a potentiometer installed on a central bar. This sensor was powered by a rechargeable battery installed on the device; so its outputs were independent of power cutoff or fluctuation. The angles measured by this sensor also were checked by manual measurements. In order to minimize the influence of the electric motor vibration on the model, the motor and gearbox were installed on the ground apart from the main body. The force required to tilt the table was transferred from the motor to the table by means of a pulley-belt system and a ball screw linear actuator. All connections of the device were equipped with rubber washers to dampen the shocks both at the start and during the test. During the tests, displacement of the model was measured by a displacement transducer installed on the box at the front of the slope. In addition, the test was video recorded from the side and front positions so that model behavior could be examined in slow-motion. To ensure the uniformity, consistence and repeatability of the method which was used to pour the powder into the box, this procedure was done by a feeder moving over adjustable rails installed above the Plexiglas box. This setup allowed the position of feeder to be adjusted both longitudinally and in height, so that powder could be poured from the desired height and at the desired position. This allowed the powder to be poured in a standard repeatable method for all models. During the tests, the feeder was removed from the device to avoid interference. As previously stated, for all models, powder was poured into the box from a fixed height of 10 cm.

For each test, first, solid blocks were placed vertically alongside each other to form the rock mass of the toe of slope. As table tilts, these blocks become susceptible to overturning. Since toppling failure of rock mass at the toe may be in blocky, flexural or block-flexure modes, each scenario was investigated separately by some models built specifically for that failure mode. For flexural toppling failure, rock mass was built

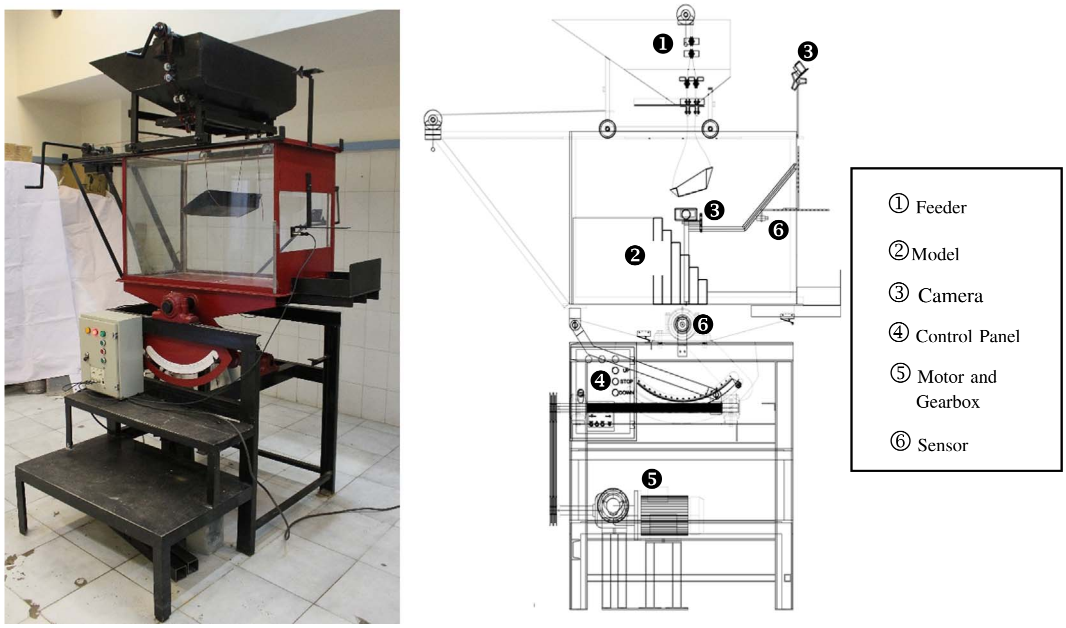

Fig. 9. Tilting table apparatus; (a) photograph, (b) schematic diagram.

with continuous blocks; so for toppling to occur, blocks had to break at the base by the tensile stress caused by bending. For blocky mode, a set of artificial cross-joint was made at the base of blocks in a way that overall toppling failure plane would be at an angle of 14° to the table floor. These joints allowed the blocks to easily separate at their bases and overturn under the exerted loads. For block-flexure toppling failure, continuous blocks and those with cross-joints were placed alternately. The dip of overall toppling failure plane was chosen to be 14° in this model too, so that block-flexure toppling failure would be regular and easier to analyze. To avoid the problems associated with making and movement of the blocks, their maximum height was limited to 35 cm. On the other hand, initial modeling showed that flexural models which were shorter than 15 cm can remain stable even under a slope angle of 90°. Therefore the height of blocks was selected between 15 cm to 30 cm for all the models with a constant block thickness of 5 cm. Furthermore, the slope angle before tilting was 56.3° for every test. After building the toe of the slope, the feeder containing the powder was fixed at the height of 10 cm from the box floor. The feeder was then moved along the container pouring a uniform layer of powder behind the rock blocks. The air pluviation process was continued for a

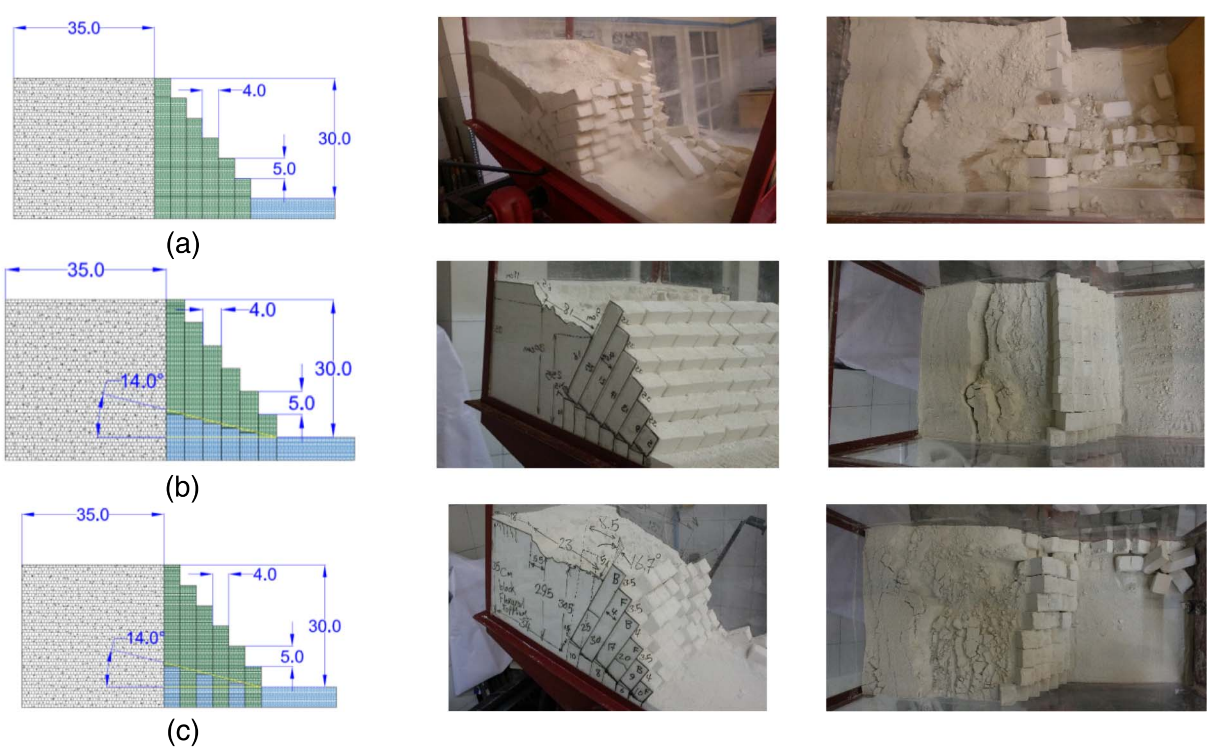

Fig. 10. Schematic diagrams and photographs of slide-toe-toppling failure in physical models; (a) flexural mode, (b) blocky mode, (c) block-flexure mode (all dimensions are in centimeter).

Table 1
Geometry of physical models at the failure stage.

Model[a]	h	ψ_f	ψ_p	ψ_b	ψ_s	ψ_t	t	b	n	Condition
	(cm)	(Degree)	(Degree)	(Degree)	(Degree)	(Degree)	(cm)	(cm)	–	
B30	32.4	64	82.3	7.7	7.7	21.7	4	20.2	6	Unstable
B25	27.3	65.8	80.5	9.5	9.5	23.5	4	22.4	5	Unstable
B20	22.1	69.3	77	13	13	27	4	17.2	4	Unstable
F30	34.7	73.3	73	17	17	27.1	4	25.1	6	Unstable
F25	29.3	79.3	67	23	23	33.36	4	18.9	5	Unstable
F20	23.3	87.3	59	31	31	42.31	4	24.5	4	Unstable
BF30	33.6	69.3	77	13	13	27	4	23	6	Unstable
BF25	28.9	76.3	70	20	20	34	4	21.1	5	Unstable
BF20	23.2	82.8	63.5	26.5	26.5	40.5	4	17.4	4	Unstable

[a] B, F, and FB denote respectively the blocky, flexural, and block-flexure modes, and the following number is the pre-tilting height of the model in centimeter.

constant powder falling height of 10 cm until the space behind the blocks was backfilled completely. Then, after checking the proper functioning of sensors and cameras, the table was tilted at a slow and continuous rate of 1° per minute. In all experiments, four stages can be considered for the tests: stable, initiation of instability, failure and post-failure. The slow rate of tilting allowed initiation of instability to be recorded. In all models, as the dip of tilting plane increased, transverse tension cracks appeared in the powder. As the test progressed, the number and depth of these cracks increased and blocks started to show deflection. In the later stages, often a number of tension cracks deepened more than others and powder-block contact surface underwent a shear displacement so that blocks could undergo bending deflection. Finally, all blocks were toppled and a roughly circular sliding occurred in the powder suddenly. This circumstance, which a large movement was observed in the model, assumed failure stage. While total movement of flexural toppling mode in failure stage was more than blocky and block-flexural modes, all models experienced self-stabilization condition in their post-failure stage. Fig. 10 shows the schematic diagrams and photographs of the models. To save space, only the diagrams and photographs of one of the typical models tested for each failure mode are presented (the model with h = 30 cm). But overall, a total of 9 physical models were conducted and their results were recorded. Geometric details of the models at the onset of failure are presented in Table 1.

In every test, tilting was stopped immediately after the failure stage, geometric details of the model were recorded, depth of sliding surface in the powder was captured three-dimensionally to acquire geometric data required for theoretical analyses and finally sliding mass and broken blocks were carefully removed to measure the height of blocks below the overall toppling failure plane (Fig. 11). To better understand the total instability surface in these models, the acquired data was tuned into 3D models. A view of one of these models (model F20) is shown in Fig. 12. As this figure shows, sliding surface in the slope's upper area is roughly circular and extends from the end of tension crack to the boundary of overall failure plane in toppling zone. It was also found that in the blocky and block-flexure models, surface of toppling failure matched the surface of cross-joints. Thus, the angle between overall toppling failure plane and the normal to discontinuities was

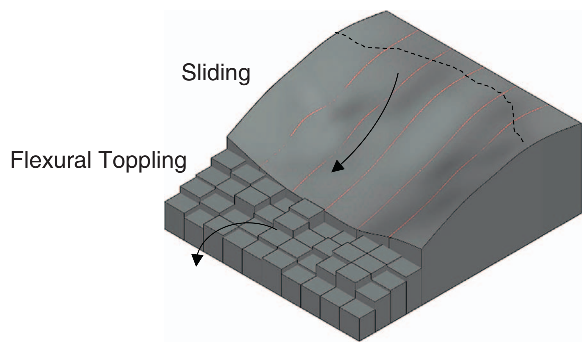

Fig. 12. 3D view of total failure plane in the model F20.

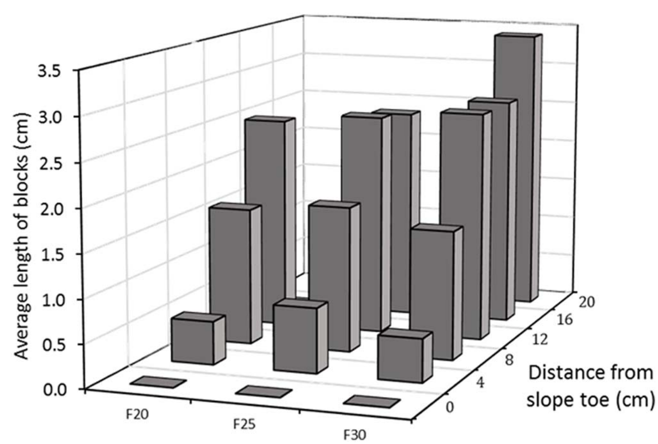

Fig. 13. 3D plot of average length of blocks below the overall toppling failure plane in flexural mode.

about 14°. But in the flexural toppling model where there was no cross-joint, failure surface had to be measured by other means. For this purpose, the average height of blocks below the total failure plane in different models was measured (Fig. 13). Then, to determine the

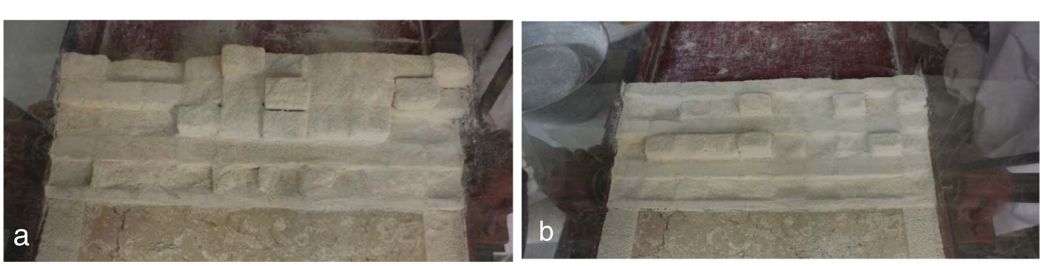

Fig. 11. A view of blocks below the total failure plane; (a) flexural toppling failure, (b) block-flexure toppling failure.

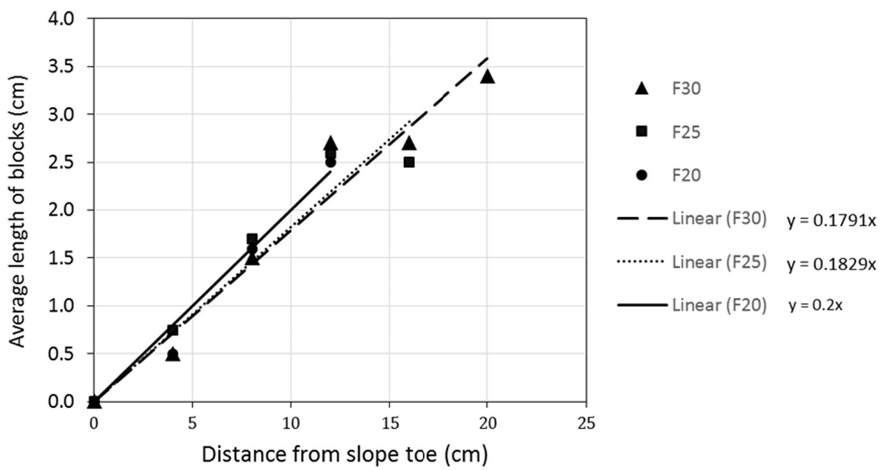

Fig. 14. Inclination of overall toppling failure plane in flexural mode.

gradient of overall failure plane, the height of these blocks was plotted versus their distance from the toe (Fig. 14). As can be seen from Figs. 13 and 14, in flexural toppling failure models, the angle between total toppling failure plane and the normal to discontinuities varied between 10° and 11.5°.

4.2. Theoretical modeling

4.2.1. Proposed theoretical model

For theoretical analysis of this type of toppling failure, first, reaction between weak material and rock masse should be determined and then applied to block “n”. In this study, this reaction force is determined by the conventional slice method. But since the contact surface between the soil and block “n” is tilted, selected slices should not be vertical. Thus, the sliding mass is divided into multiple hypothetical slices, all parallel to dominant discontinuities of the rock mass. A random sliding surface is assumed in soil mass to ensure the adequate generality of sliding surface geometry and thus its capability to account for various circular and non-circular forms. Fig. 15 shows a diagram of this slicing and the forces exerted on a typical slice (slice “j”) of sliding mass. As this figure shows, free body diagram of each slice has 9 unknowns ($f_R^j, f_L^j, N^j, S^j, \psi_R^j, \psi_L^j, h_R^j, h_L^j, \ell^j$), thus, the total number of unknowns for sliding mass is 9m. If we remove the unknowns shared between slices ($f_L^j = f_R^{j+1}, \psi_L^j = \psi_R^{j+1}, h_L^j = h_R^{j+1}$), ignore the unknowns of right side of slice “1” according to boundary conditions ($f_R^1 = h_R^1 = \psi_R^1 = 0$), assume the sliding mass to be in limit equilibrium condition ($S^j = N^j \tan\phi_s + c_s\Delta x^j/\sin(\psi_a^j + \psi_p)$) and assume that the vertical force acting on the base of each slice to be applied to the center of its bottom ($\ell^j = \Delta x^j/2$), the number of unknowns will be reduced to 4m. Nevertheless, we have access to only 3m equilibrium equations (2m forces equilibrium equations and m moments equilibrium equations); so the sliding mass is statically indeterminate and should be simplified and analyzed with an appropriate technique for this purpose. In this research, the inter-slice forces and their points of application are determined by the following procedure.

According to Fig. 15, writing the forces equilibrium equations along x and y axes for slice “j” gives:

$$\sum f_y^j = 0 \rightarrow f_L^j \cos\psi_L^j + S^j \sin(\Psi^j) + N^j \cos(\Psi^j) - W^j \cos\psi_p - f_R^j \cos\psi_R^j = 0 \tag{3}$$

$$\sum f_x^j = 0 \rightarrow f_L^j \sin\psi_L^j - S^j \cos(\Psi^j) + N^j \sin(\Psi^j) - W^j \sin\psi_p - f_R^j \sin\psi_R^j = 0 \tag{4}$$

where $\Psi^j = \psi_a^j + \psi_p$.

Assuming that sliding mass is in the limit equilibrium condition and follows the Mohr-Coulomb failure criterion, the normal and shear forces acting on the slice bottom will have the following relationship:

$$S^j = N^j \tan\phi_s + c_s \frac{\Delta x^j}{\sin(\Psi^j)} \tag{5}$$

Determining S^j by Eq. (5) and substituting its value into Eqs. (3) and (4) and, then, substituting the N^j obtained from Eq. (3) into Eq. (4) result in the following relationship for f_L^j:

$$\begin{aligned}
f_L^j &= \frac{f_R^j \xi_1^j + W^j \xi_2^j + c^j \xi_3^j}{\xi_4^j} \\
\xi_1^j &= \cos\psi_R^j [\sin\Psi^j - \cos\Psi^j \tan\phi_s] - \sin\psi_R^j [\cos\Psi^j + \sin\Psi^j \tan\phi_s] \\
\xi_2^j &= \cos\psi_p [\sin\Psi^j - \cos\Psi^j \tan\phi_s] - \sin\psi_p [\cos\Psi^j + \sin\Psi^j \tan\phi_s] \\
\xi_3^j &= \frac{-\Delta x^j}{\sin(\Psi^j)} \\
\xi_4^j &= \cos\psi_L^j [\sin\Psi^j - \cos\Psi^j \tan\phi_s] - \sin\psi_L^j [\cos\Psi^j + \sin\Psi^j \tan\phi_s]
\end{aligned} \tag{6}$$

Also, writing the moment equilibrium equation with respect to middle point of base of the slice “j” gives:

$$\begin{aligned}
\sum M = 0 \rightarrow\ & f_R^j \cos\psi_R^j (h_R^j + 0.5\Delta x^j \tan(\Psi^j - 90)) \\
& - f_L^j \cos\psi_L^j (h_L^j - 0.5\Delta x^j \tan(\Psi^j - 90)) \\
& - 0.5 f_R^j \sin\psi_R^j \Delta x^j - 0.5 f_L^j \sin\psi_L^j \Delta x^j + 0.5\, W^j \cos\psi_p h^j = 0
\end{aligned} \tag{7}$$

After arranging Eq. (7), h_L^j will be given by:

$$h_L^j = \frac{\begin{aligned} & 0.5\, W^j \cos\psi_p h^j + f_R^j \cos\psi_R^j h_R^j \\ & - 0.\ 5\Delta x^j (\sin\psi_R^j f_R^j + \sin\psi_L^j f_L^j - \tan(\Psi^j - 90)(\cos\psi_R^j f_R^j \\ & + \cos\psi_L^j f_L^j)) \end{aligned}}{f_L \cos\psi_L} \tag{8}$$

To solve the problem, we assume a primary function such as $\psi^j = \kappa F(x_j)$ for the angles of inter-slice forces; where $F(x_j)$ is a function with the range (0–1), κ is a positive constant and x_j is the distance of lower left corner of slice j from the point where sliding surface coincides with block “n” (point O in Fig. 15). Some functions that are typically used as $F(x_j)$ are shown in Fig. 16. At the moment of failure, we observed tension cracks behind the crown of the slope; so the value of this function for the right side of slice “1” is zero. The physical models showed that for toppling failure to be occurred, block “n” and slice “m” have to slide against each other so that this block would be able to overturn about its base. Thus, if we ignore the cohesive strength between these two elements (rock block “n” and soil slice “m”), then $\psi_L^m = \phi_{sb}$. Therefore, it can be concluded that in the analysis of sliding mass shown in Fig. 15, $F(x_j)$ of the right side of slice “1” is zero while that of the left side of slice “m” is nonzero (ϕ_{sb}). Thus, it is better to define inter-slice forces with clipped half-sine function. The mathematical relationship of this function is expressed with:

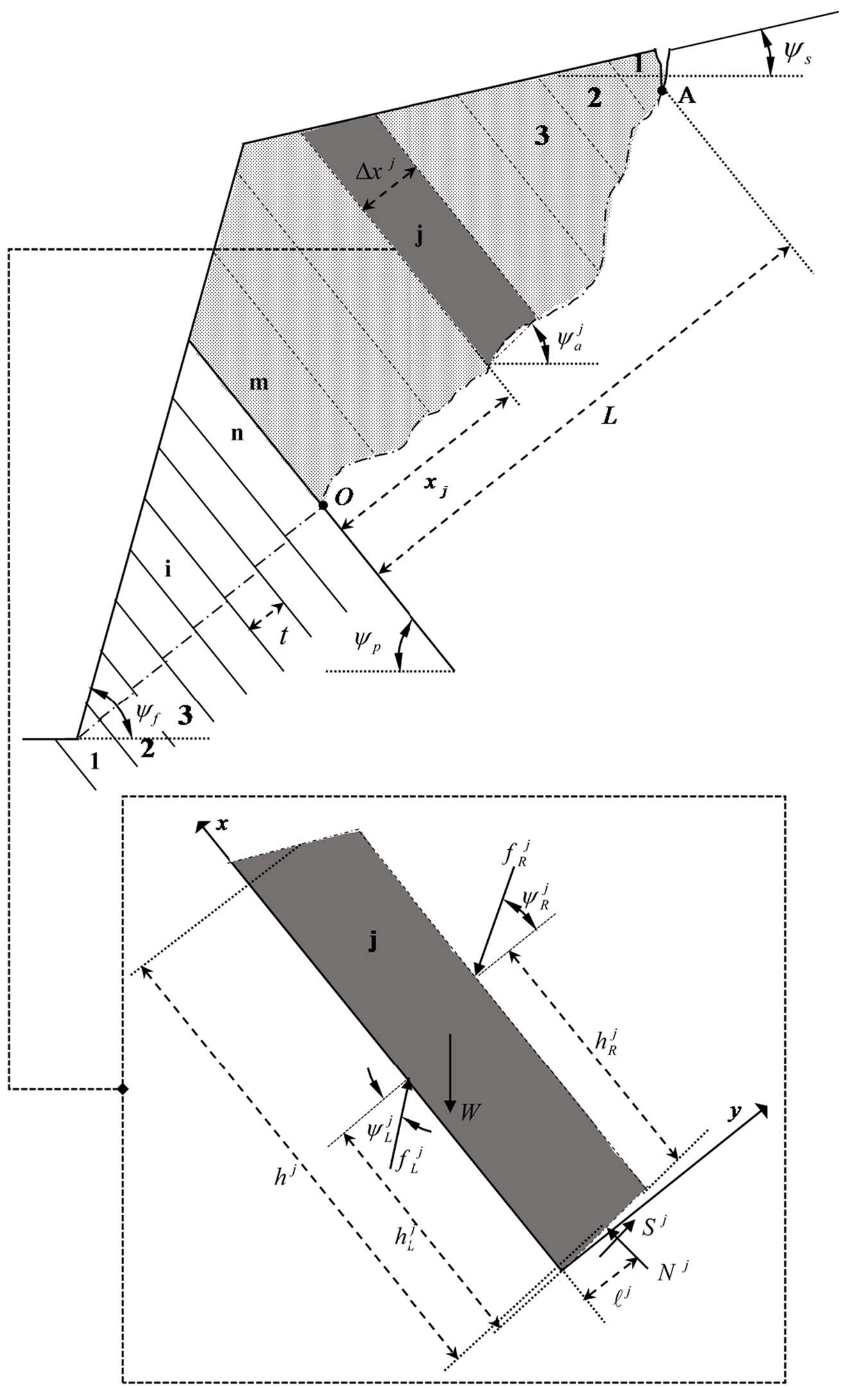

Fig. 15. A schematic view of slide-toe-toppling failure and forces acting on a given slice of the soil mass with the sliding potential.

$$\psi^j = \kappa \sin\left[\left((1-a)\frac{x_j}{L} + a\right)\pi\right] \tag{9}$$

where a is a constant coefficient chosen between 0 and 1 and κ is determined according to a and boundary conditions. The angle ψ^j must be smaller than or equal to ϕ_s (inter-slice friction angle). Also, L denotes the direct distance between the point O and the end of tension crack (the point A). For example, if we assume a friction angle of 32° between the slice "m" and the block "n" and an internal friction angle of 38° for the soil, curves of function ψ^j for different values of a will be plotted in Fig. 17.

To solve the problem, first, a is initialized with a primary value and force $f_R^{\,1}$ is assumed to be zero. With these values at hand, force $f_L^{\,1}$ can be obtained from Eq. (6). Since $f_R^{\,2} = f_L^{\,1}$, the recently obtained value can be substituted into Eq. (6) as a replacement for $f_R^{\,2}$ in order to obtain $f_L^{\,2}$. The same process can be repeated until slice "m". Then, a can be adjusted in a way that force $f_L^{\,m}$ (interaction between soil slice "m" and rock block "n") becomes maximum. Doing so gives all the inter-slice forces as well as the interaction forces between sliding mass and rock mass with potential of toppling failure. Depending on the sign of force $f_L^{\,m}$, one of the following states will occur:

- $f_L^{\,m} \le 0$: sliding mass is stable or at the point of equilibrium and thus there are no external forces being applied to the rock mass at the toe of the slope. Therefore, the slope will be stable against slide-toe-toppling failure.
- $f_L^{\,m} > 0$: slope has a potential of slide-toe-toppling failure, as the reaction of this force functions as an external force acting on block "n" and contributing to toppling failure. In this case, with the

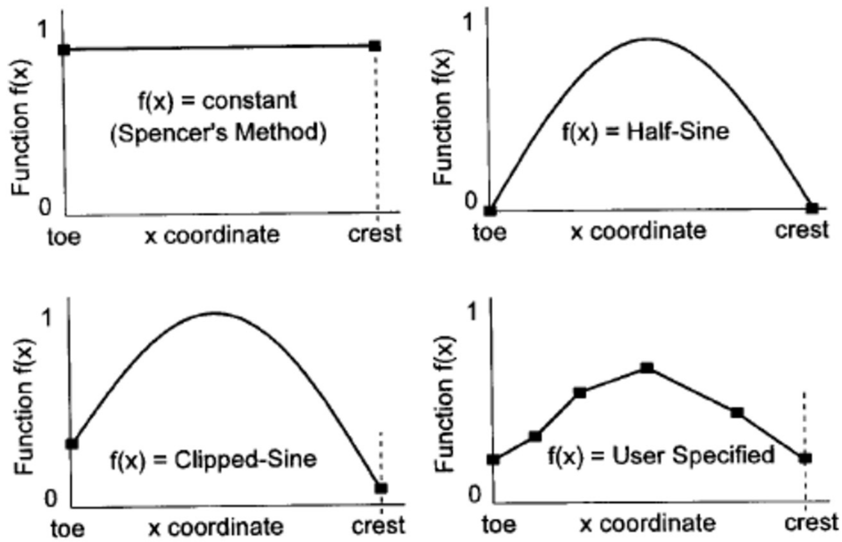

Fig. 16. Typical functions for determination of inter-slice forces in general circular and non-circular sliding shapes (Abramson et al., 2002).

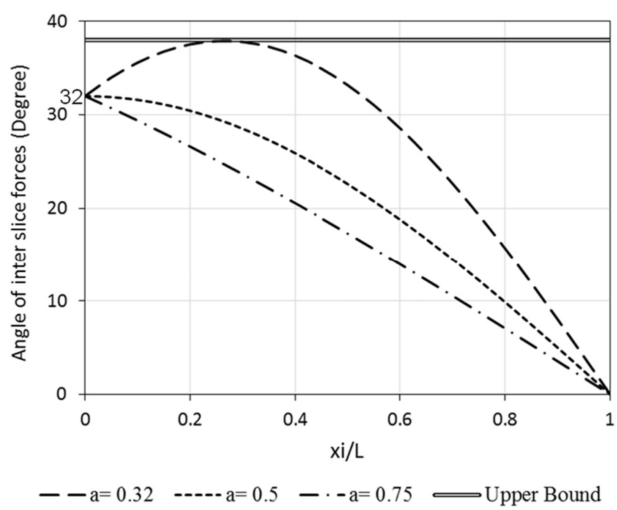

Fig. 17. Functions of inter-slice forces for a typical example.

boundary condition of slice “1” in mind, the point of application of the force acting on its right side ($h_R{}^1$) can be equated to zero so that the point of application of the force acting on its left side ($h_L{}^1$) can be calculated by Eq. (8) and the same process can be continued until slice “m”. This procedure gives the point of application of interaction force between sliding mass and the rock block “n”.

According to Figs. 15 and 18, rock mass constituting the toe of mentioned slopes are prone to blocky, flexural or block-flexure toppling failures. So in general, a rock block in the toppling zone undergoes sliding, toppling, bending or shearing, in which case, the force acting on the right side of this block can be obtained, respectably, from the following relationships (Amini et al., 2012):

$$P_{i-1,s} = P_i + \frac{W_i(\sin\psi_b - \cos\psi_b\tan\phi_b) - c_b t}{1 - \tan\phi_b\tan\phi_c} \tag{10}$$

$$P_{i-1,t} = \frac{P_i[y_i - \tan\phi_c \mathrm{t}] + 0.5W_i[\sin\psi_b h_i - \cos\psi_b \mathrm{t}]}{y_{i-1}} \tag{11}$$

$$P_{i-1,f} = \frac{P_i(y_i - 0.5\tan\phi_c \mathrm{t}) + 0.5W_i\sin\psi_b h_i - \frac{2I}{t}\left(\sigma_t + \frac{W_i\cos\psi_b}{t}\right)}{y_{i-1} + 0.5\tan\phi_c \mathrm{t}} \tag{12}$$

$$P_{i-1,sh} = P_i + \frac{W_i(\sin\psi_b - \cos\psi_b\tan\varphi_i) - c_i t}{1 - \tan\phi_c\tan\phi_i} \tag{13}$$

The presence of a cross-joint at the block base undermines its ability to resist against bending stress; so it either topples or slides, in which case, sliding or overturning can be examined by Eqs. (10) and (11). If $P_{i-1,s} > P_{i-1,t}$, rock block has the potential of sliding failure; but if $P_{i-1,t} > P_{i-1,s}$, toppling has a stronger possibility. If both of these forces are negative, this block is stable and applies no force to the next block ($P_{i-1} = 0$). A block that is cantilever is subjected to bending stresses; so it may break under bending-induced tensile stress or undergo shearing due to the resultant of forces acting on it, in which case, its stability status can be determined by Eqs. (12) and (13). Here, if $P_{i-1,f} > P_{i-1,sh}$ rock block has the potential of bending; but if $P_{i-1,sh} > P_{i-1,f}$ shearing has a stronger possibility. As before, if both of these forces are negative, this block is stable and applies no force to the next block. In all these cases, it is assumed that shear stresses exerted on the sides of each block (Q_i) can be determined by the Mohr-Coulomb failure criterion. In any case, when the block “n” is cantilever or has cross-joint at its base, reaction force between sliding mass and rock mass ($f_L{}^m$) can be substituted into the mentioned relations to determine the force acting on the left side of the block “n” and the inter-block forces can be calculated in the same manner in order to ultimately determine the force required for the rock block “1” to remain stable. The sign of this force can be used to evaluate the overall stability of the slope against slide-toe-toppling failure:

- $P_0 > 0 \rightarrow$ Slope is unstable.
- $P_0 < 0 \rightarrow$ Slope is stable.
- $P_0 = 0 \rightarrow$ Slope is at the point of equilibrium.

Moreover, shear parameters of discontinuities, intact rock and sliding surface can be adjusted in a way that slope would reach the point of equilibrium and then the obtained shear parameters can be compared with the real values to determine the slope's FoS against slide-toe-toppling failure. This technique is a common practice for determination of the slope's FoS. In all discussed calculations, it is assumed that the slope is completely dry and is subjected to no external forces such as dynamic and structural loads or reinforcement force. When the slope's water level is higher than overall failure plane or sliding surface or when the slope is subjected to some external loads, these forces can be added to the discussed limit equilibrium equations to reanalyze the situation. Since magnitude and point of application of these forces are known, they make no change in general condition and structure of the solution.

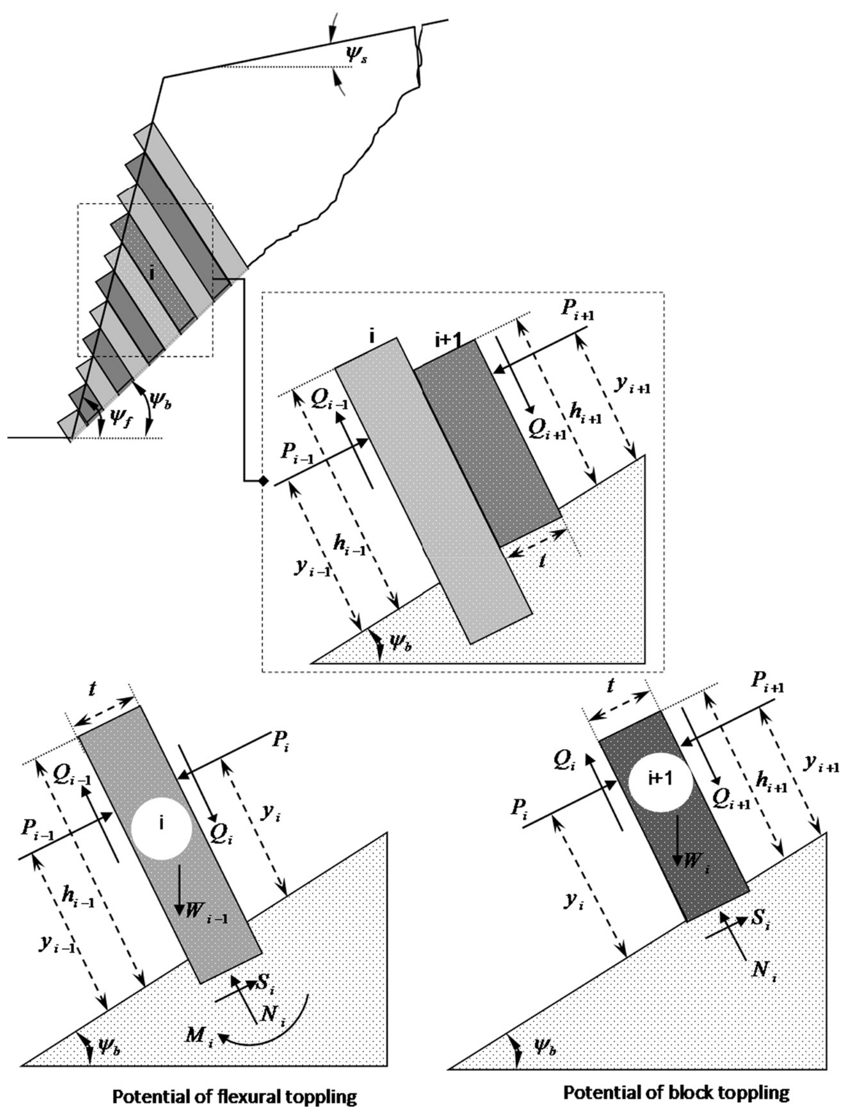

Fig. 18. Analysis of slide-toe-toppling failure.

4.3. Analysis of a typical example with the proposed theoretical method

Analysis of physical models or real case studies with a potential of slide-toe-toppling failure with the proposed theoretical method requires extensive calculations which would take considerable time and effort to be performed manually. To avoid manual calculations, the proposed theoretical method for analysis of slide-toe-toppling failure was coded into a computer program. This program receives the slope's characteristics from the user and performs all analyses associated with the proposed method and displays all geometric information and forces acting on rock blocks and soil slices. This program allows the user to adjust the values of parameters and thereby examine the sensitivity of the slope to different variables. To evaluate the performance of the proposed method, the coded program was used to analyze a typical example. To

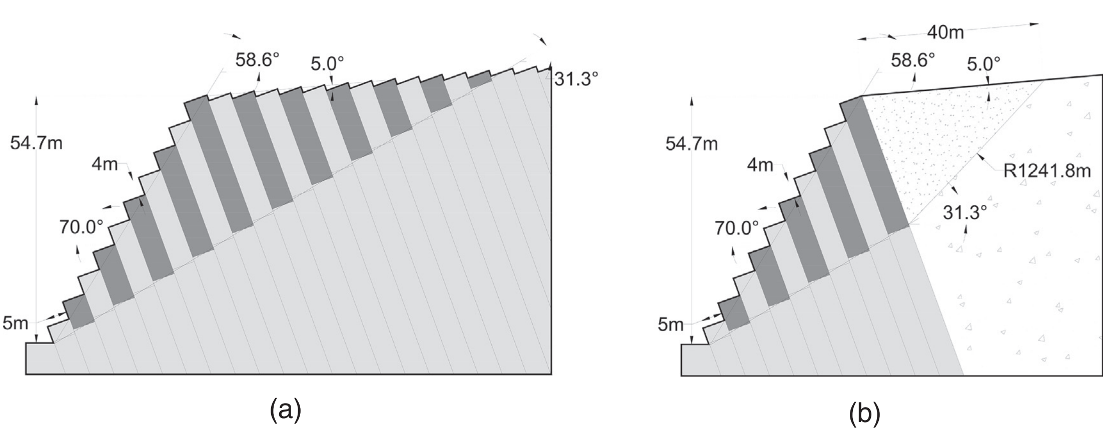

Fig. 19. Diagrams of the studied typical examples; (a) main toppling failure, (b) secondary toppling failure.

Table 2
Results of stability analysis of a typical example against slide-toe-toppling and main toppling failures.

Geotechnical specifications of materials

Unit weight of soil (N/m^3)	Cohesive strength of soil (Pa)	Friction angle of soil (Degree)	Unit weight of blocks (N/m^3)	Cohesive strength of blocks (Pa)	Friction angle of base of blocks (Degree)	Friction angle between blocks (Degree)	Friction angle of intact rock (Degree)	Tensile strength of intact rock (Pa)
25,000	5000	32	27,000	20,000,000	35	30	35	3,500,000

Geometrical specifications of main toppling failures

Number of blocks	Dip of blocks (Degree)	Dip of face slope (Degree)	Dip of upper surface (Degree)	Dip of basal plane (Degree)	Thickness of columns (m)	Height of slope (m)	Dip of normal to discontinuities (Degree)
22	70.00	58.66	5.00	31.31	5.00	54.69	20.00

Geometrical specifications of slide-toe-toppling failure

Number of blocks	Number of slices	Dip of blocks (Degree)	Dip of face slope (Degree)	Dip of upper surface (Degree)	Dip of basal plane (Degree)	Thickness of columns (m)	Height of slope (m)	Location of tension crack (m)
10	10	70.00	58.66	5.00	31.31	5.00	54.69	40.00

Main toppling failures

Toppling	Column no.	Height (m)	Blocky Force (kN)	Failure mode	Flexural Force (kN)	Failure mode	Block-Flexure Force (kN)	Failure mode
	22	2.42	0.00	Stable	0.00	Stable	0.00	Stable
	21	4.76	0.00	Stable	0.00	Stable	0.00	Stable
	20	7.10	0.00	Stable	0.00	Stable	0.00	Stable
	19	9.44	0.00	Stable	0.00	Stable	0.00	stable
	18	11.78	0.00	Stable	0.00	Stable	0.00	Stable
	17	14.12	8.88	Toppling	0.00	Stable	0.00	Stable
	16	16.46	69.49	Toppling	0.00	Stable	62.89	Toppling
	15	18.80	170.77	Toppling	0.00	Stable	0.00	Stable
	14	21.14	307.56	Toppling	0.00	Stable	170.92	Toppling
	13	23.48	477.14	Toppling	0.00	Stable	0.00	Stable
	12	25.82	677.99	Toppling	0.00	Stable	278.96	Toppling
	11	28.16	909.21	Toppling	33.12	Flexural	346.86	Flexural
	10	30.50	1346.84	Toppling	204.20	Flexural	697.15	Toppling
	9	27.50	1782.45	Toppling	206.44	Flexural	950.99	Flexural
	8	24.50	2176.20	Toppling	13.75	Flexural	1027.04	Toppling
	7	21.50	2534.81	Toppling	0.00	Stable	989.44	Flexural
	6	18.50	2869.70	Toppling	0.00	Stable	907.15	Toppling
	5	15.50	3202.34	Toppling	0.00	Stable	206.19	Flexural
	4	12.50	3579.75	Toppling	0.00	Stable	121.45	Toppling
	3	9.50	4135.35	Toppling	0.00	Stable	0.00	Stable
	2	6.50	5542.39	Toppling	0.00	Stable	0.00	Stable
	1	3.50	5291.79	Sliding	0.00	Stable	0.00	Stable
	–	–	–	–	–	–	–	–
	–	–	–	–	–	–	–	–
	–	–	–	–	–	–	–	–
	–	–	–	–	–	–	–	–
	–	–	–	–	–	–	–	–

Slide-toe-toppling failure

Sliding	a	Coordinate of failure plane center X (m)		Y (m)	Failure plane radius (m)
	0.9	− 849.03		889.86	1241.82
	Slice no.	Height (m)	Weight (kN)	ψi (Degree)	Point of application (m)	Force (kN)
	1	1.54	148.60	3.25	2.67	22.25
	2	4.61	444.98	6.50	4.23	125.86
	3	7.66	739.68	9.75	5.86	311.77
	4	10.69	1032.72	12.98	7.41	582.72
	5	13.71	1324.10	16.20	8.83	943.38
	6	16.71	1613.85	19.40	10.13	1400.53
	7	19.69	1901.95	22.59	11.29	1963.38
	8	22.66	2188.43	25.75	12.31	2643.99
	9	25.61	2473.30	28.89	13.16	3457.86
	10	28.54	2756.55	32.00	13.84	4424.69

Interaction	Inclination (Degree)	Point of application (m)	Force (kN)
	32.00	13.84	4424.69

Toppling	Column no.	Height (m)	Blocky Force (kN)	Failure mode	Flexural Force (kN)	Failure mode	Block-Flexure Force (kN)	Failure mode
	10	30.50	2441.55	Toppling	2952.99	Flexural	2441.55	Toppling
	9	27.50	2929.03	Toppling	3007.60	Flexural	3334.69	Flexural
	8	24.50	3385.04	Toppling	2875.40	Flexural	2857.06	Toppling
	7	21.50	3820.55	Toppling	2522.58	Flexural	3508.87	Flexural
	6	18.50	4254.16	Toppling	1895.76	Flexural	2859.83	Toppling
	5	15.50	4720.82	Toppling	903.86	Flexural	2932.37	Flexural
	4	12.50	5297.10	Toppling	0.00	Stable	2282.58	Toppling
	3	9.50	6200.31	Toppling	0.00	Stable	877.42	Flexural
	2	6.50	8526.88	Toppling	0.00	Stable	412.02	Sliding
	1	3.50	8276.28	Sliding	0.00	Stable	0.00	Stable

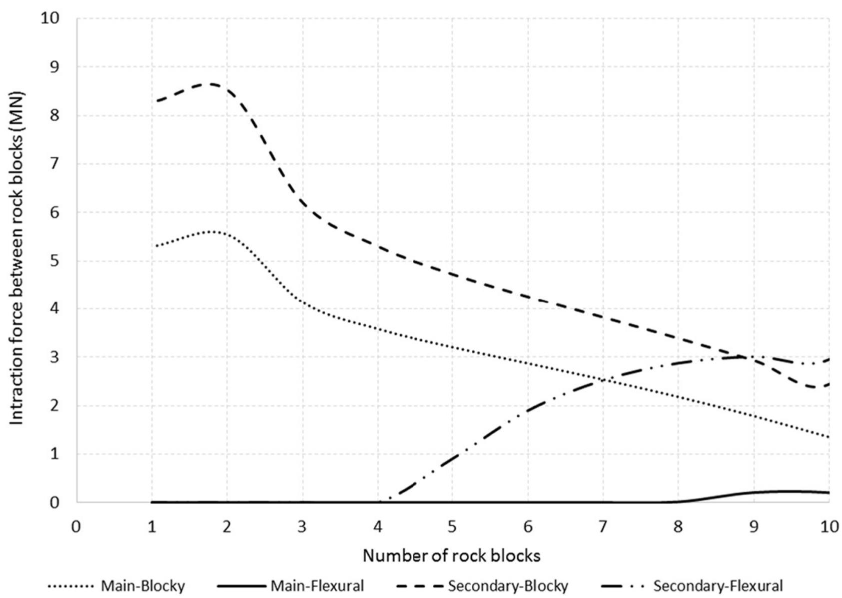

Fig. 20. Magnitudes of inter-column normal forces acting at rock blocks in the toe of the slopes.

allow the readers to compare the slide-toe-toppling failure with the main toppling failures, this example was also analyzed for the main flexural, blocky and block-flexure toppling failures. The diagram of one state of this example is illustrated in Fig. 19. The analyses for the main flexural, blocky, and block-flexure toppling failures were performed by the methods of Goodman and Bray (1976), Aydan and Kawamoto (1992) and Amini et al. (2012), respectively. The results of different analyses on this example are presented in Table 2. Geometrical and geotechnical specifications of the slope which are fed to the program as inputs are displayed in the top section of the table and the results of analyses for different failures are shown in the bottom section. The left side of this table shows the results of stability analysis of the example against the main toppling failures. As can be seen, this slope is unstable against blocky toppling failure; because block 1 slides and blocks 2 to 17 topple. Note that in this case, a stable zone appears behind the crown of the slope (blocks 18 to 22). The analyses also show that this example is perfectly stable against flexural toppling failure. In this case, reactions are limited between the blocks 8 to 11 and other blocks apply no force to each other; so the slope as a whole can be considered stable against this mode of failure. The last two columns of this section of the table show the results of stability analysis of the slope against block-flexure toppling failure. These results show that the slope is also stable against block-flexure mode; but not as strongly as against flexural toppling failure. Because this stability relies only on stability of blocks 1 to 3 while blocks 4 to 12 have inter-block reactions. The analysis also indicates that blocks 14 and 16 tend to undergo blocky toppling; but are stabilized by blocks 13 and 15, respectively. The right side of the table displays the results of stability analysis of the example against slide-toe-toppling failure. In this part of the table, the results are partitioned into two sections. The upper section is dedicated to the result pertaining to circular sliding in soil mass. As can be seen, all inter-slice forces are positive which indicates that soil has a circular sliding potential. The reaction between soil and rock mass is equal to the force exerted on slice 10 which has a magnitude of 4424.69 kN and is applied to a point located 13.84 m above the base of this slice. Applying this force to block 10 allows the toe of the slope to be analyzed for flexural, blocky and block-flexure toppling modes. The results of these analyses are displayed below this section. These results show that if the toe has a potential of blocky toppling failure, the slope will not be stable against slide-toe-toppling; because block 1 will slide and blocks 2 to 10 will topple. But if the toe has a potential of flexural toppling failure, the slope as a whole will be stable against slide-toe-toppling failure; because a stable zones appearing in the toe (blocks 1 to 4) will stabilize the entire mass. The last column of this section shows that if the toe has a potential of block-flexure toppling failure, the slope will be at the point of instability and the smallest external force (e.g. earthquake or underground water pressure) can make it unstable. This is because, in this case, stability of the entire mass only relies on the stability of block 1 as other blocks have a tendency to slide or topple.

For more explanation, magnitudes of inter-column normal forces acting at rock blocks in the toe of these case studies are presented in Fig. 20. Although, to clarify the figure, outcomes of blocky and flexural modes are shown in the figure, block-flexural one has also similar results. As can be seen from the graph, magnitude of the force in

Table 3
Geometry of theoretical models at the moment of failure.

Model[a]	ψ_f	ψ_p	ψ_b	ψ_s	ψ_t	t	b	n	Condition
	(Degree)	(Degree)	(Degree)	(Degree)	(Degree)	(cm)	(cm)	–	
B30	65.11	81.19	8.81	8.81	22.81	4	20.2	6	Limit equilibrium
B25	67.13	79.17	10.83	10.83	24.83	4	22.4	5	Limit equilibrium
B20	69.97	76.33	13.67	13.67	27.67	4	17.2	4	Limit equilibrium
F30	71.18	75.12	14.88	14.88	24.98	4	25.1	6	Limit equilibrium
F25	76.71	69.59	20.41	20.41	30.77	4	18.9	5	Limit equilibrium
F20	86.13	60.17	29.83	28.37	39.68	4	24.5	4	Limit equilibrium
BF30	69.47	76.83	13.17	13.17	27.17	4	23	6	Limit equilibrium
BF25	73.39	72.91	17.09	17.09	31.09	4	21.1	5	Limit equilibrium
BF20	79.22	67.08	22.92	22.92	36.92	4	17.4	4	Limit equilibrium

[a] B, F, and FB denote respectively the blocky, flexural, and block-flexure modes, and the following number is the pre-tilting height of the model in centimeter.

Table 4
Comparison of experimental results with the predictions of the proposed theoretical method.

Models	B30	B25	B20	F30	F25	F20	BF30	BF25	BF20
Experimental measurements (Degree)	7.7	9.5	13	17	23	31	13	20	26.5
Theoretical predictions (Degree)	8.81	10.83	13.67	14.88	20.41	28.37	13.17	17.09	22.92
Errors%	14.42	14	5.15	− 12.47	− 11.26	− 12.39	1.31	− 14.55	− 13.51

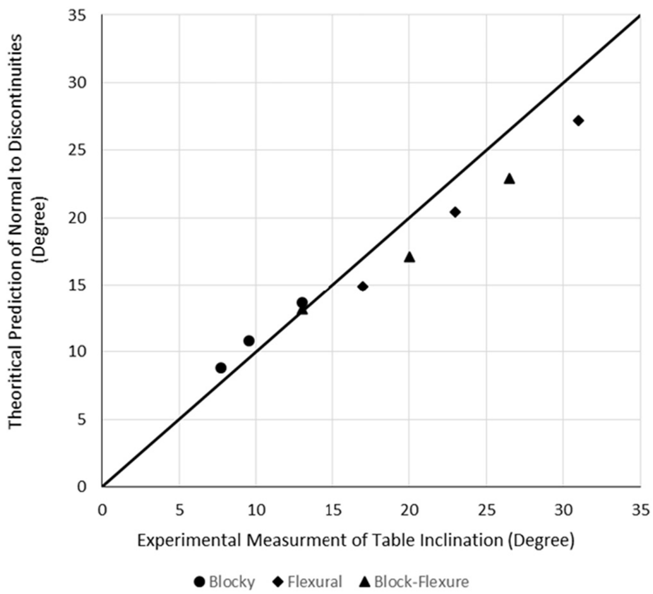

Fig. 21. Comparison of experimental results with the predictions of the proposed theoretical method.

secondary mode is more than main toppling failure for all rock blocks. But, general trend of this force is similar in main and secondary ones.

4.4. Analysis of physical models with the proposed theoretical method

To verify the results of the proposed method, this method was used to analyze the physical models described in Section 4.1. In these analyses, physical and mechanical properties of soil and rock materials were assumed as described in Section 4.1.1. Limit equilibrium conditions of the models were determined with the proposed theoretical method and the results of physical and theoretical models were subjected to quantitative comparison. Table (3) presents the predictions of the proposed theoretical method regarding the geometry of physical models under limit equilibrium condition.

5. Comparison of physical and theoretical results

In Section 4.4, the proposed theoretical method was used to analyze the physical slide-toe-toppling models and predict their geometry at the moment of failure. Thus, the error of theoretical approach can be determined by comparing these results (Table 3) with the real geometry observed in physical models (Table 1). This comparison can be made based on several parameters; but since tilting table of the physical models had a varying inclination, the angle of inclination was selected as the basis of this comparison. In the theoretical models, the angle of the line normal to dominant discontinuities matches the table's angle of inclination. So the error of the proposed theoretical method can be determined by comparing this angle with the table's angle of inclination in observations. In Table 4, these two parameters are compared and the errors of the theoretical approach are reported. As it can be seen, in all cases, the error of the proposed theoretical method in prediction of table's angle of inclination at the moment of failure is < 15%. With respect to the complexity of the mechanism of this failure, these errors may be reasonable. These two parameters (table's real inclination angle at the moment of failure in the physical models and the angle of the line normal to dominant discontinuities in the theoretical models) are also compared in Fig. 21. Similar to Table 4, this plot also shows a satisfactory agreement between the theoretical and experimental results.

6. Conclusions

In this study, the mechanism of slide-toe-toppling failure was investigated through a series of physical models. The investigation results showed that a roughly circular failure in the homogeneous soil mass at the upper part of the slope leads to toppling failure of the rock blocks at the toe of the slope. This observed mechanism was used as a base to develop a theoretical model for the analysis of this type of slope instability. In the resulting model, first, the reaction forces between soil and rock mass are obtained by limit equilibrium methods. Then the obtained force is transferred to the rock mass at the toe to determine its stability against toppling failure. The validity of this theoretical method was investigated by comparing its results with the experimental observations. The results showed a difference of < 15% between the theoretical predictions and the experimental results. Considering the complexity of the mechanism of the failure, this level of error is reasonable.

Acknowledgment

The authors express their sincere thanks to Prof. Ömer Aydan from Ryukyu University, Ryukyu, Japan for his invaluable help and guidance throughout this research.

This research did not receive any specific grant from funding agencies in the public, commercial, or not-for-profit sectors.

References

Abramson, L.W., Lee, T.S., Sharma, S., Boyce, G.M., 2002. Slope Stability and Stabilization Methods, second ed. John Wiley Sons, Inc.
Adhikary, D.P., Guo, H., 2002. An orthotropic Cosserat elasto-plastic model for layered rocks. Rock Mech. Rock. Eng. 35, 161–170.
Adhikary, D.P., Dyskin, A.V., Jewell, R.J., Stewart, D.P., 1997. A study of the mechanism of flexural toppling failure of rock slopes. Rock Mech. Rock. Eng. 30, 75–93.
Alejano, L.R., Carranza-Torres, C., Giani, G.P., Arzúa, J., 2015. Study of the stability against toppling of rock blocks with rounded edges based on theoretical and experimental approaches. Eng. Geol. 195, 172–184.
Alzo'ubi, A.K., Martin, C.D., Cruden, D.M., 2010. Influence of tensile strength on toppling failure in centrifuge tests. Int. J. Rock Mech. Min. Sci. 47, 974–982.
Amini, M., 2014. Analysis of Some Secondary Toppling Failures in Rock Slopes. In: Interim Report, October 12 Rock Mechanics and Rock Engineering Department, Tehran University (35 pp.).
Amini, M., Majdi, A., Aydan, Ö., 2009. Stability analysis and the stabilization of flexural toppling failure. Rock Mech. Rock. Eng. 42, 751–782.
Amini, M., Majdi, M., Veshadi, M.A., 2012. Stability analysis of rock slopes against block-flexure toppling failure. Rock Mech. Rock. Eng. 45, 519–532.
Amini, M., Gholamzadeh, M., Khosravi, M.H., 2015. Physical and theoretical modeling of rock slopes against block-flexure toppling failure. Int. J. Min. Geol. Eng. 49, 155–171.
Ashby, J., 1971. Sliding and Toppling Modes of Failure in Models and Jointed Rock Slopes. (M Sc thesis) Imperial College, University of London.
Aydan, Ö., Amini, M., 2009. An experimental study on rock slopes against flexural toppling failure under dynamic loading and some theoretical considerations for its stability assessments. J. Sch. Mar. Sci. Technol. Tokai Univ. 7, 25–40.
Aydan, Ö., Kawamoto, T., 1992. Stability of slopes and underground openings against flexural toppling and their stabilization. Rock Mech. Rock. Eng. 25, 143–165.
Bobet, A., 1999. Theoretical solutions for toppling failure. Int. J. Rock Mech. Min. Sci. 36, 971–980.
Brideau, M., Stead, D., 2010. Controls on block toppling using a three dimensional

distinct element approach. Rock Mech. Rock. Eng. 43, 241–260.
Choquet, P., Tanon, D.D.B., 1985. Nomograms for the Assessment of Toppling Failure in Rock Slopes. In: 26th US Symposium on Rock Mechanics, Rapid Citypp. 19–30.
Cundall, P., 1971. A Computer Model for Simulating Progressive, Large Scale Movements in Blocky Rock Systems. Proc Int Symp on Rock Fracture Nancy, France, Paper 11–8.
De Freitas, M.H., Watters, R.J., 1973. Some field examples of toppling failure. Geotechnique 23, 495–514.
Egger, P., 1983. A New Development in the Base Friction Technique. In: Coll. Phys. Geomech. Models ISMES, Bergamo, pp. 67–87.
Goodman, R.E., Bray, J.W., 1976. Toppling of Rock Slopes. ASCE Specialty Conference on Rock Engineering for Foundations and Slopes, Boulder Colorado 2. pp. 201–234.
Hoek, E., Bray, J., 1977. Rock Slope Engineering, first ed. IMM, London.
Kawamoto, T., Obara, Y., Ichikawa, Y., 1983. A base friction apparatus and mechanical properties of a model material (in Japanese). J. Min. Metall. Inst. of Japan 99, 1–6.
Khosravi, M.H., Takemura, J., Pipatpongsa, T., Amini, M., 2016. In-flight excavation of slopes with potential failure planes. J. Geotech. Geoenviron. Eng. 142 (5). http://dx.doi.org/10.1061/ (ASCE) GT.1943-5606.0001439.
Majdi, A., Amini, M., 2010. Analysis of geo-structural defects in flexural toppling failure. In. J. Rock Mech. Min. Sci. 48, 175–186.
Mohtarami, E., Jafari, A., Amini, M., 2014. Stability analysis of slopes against combined circular–toppling failure. Int. J. Rock Mech. Min. Sci. 67, 43–56.
Müller, L., 1968. New considerations on the Vaiont slide. Rock Mech. Eng. Geol. 6, 1–91.
Naresh, K.T., Shuichiro, Y., Osamu, O., 2002. A toppled structure with sliding in the Siwalik Hills, midwestern Nepal. Eng. Geol. 64, 339–350.
Pritchard, M.A., Savigny, K.W., 1990. Numerical modelling of toppling. Can. Geotech. J. 27, 823–834.
Sagaseta, C., Sánchez, J.M., Cañizal, J., 2001. A general solution for the required anchor force in rock slopes with toppling failure. Int. J. Rock Mech. Min. Sci. 38, 421–435.
Smith, J.V., 2015. Self-stabilization of toppling and hillside creep in layered rocks. Eng. Geol. 196, 139–149.
Tatone, Brayan S.A., Grasselli, G., 2010. ROCKTOPPLE: a spreadsheet-based program for probabilistic block-toppling analysis. Comput. Geosci. 36, 98–114.
Teme, S.C., West, T.R., 1983. Some Secondary Toppling Failure Mechanism in Discontinuous Rock Slopes. 24th U.S. Symposium on Rock Mechanicspp. 193–204.
Wyllie, D.C., Mah, C.W., 2004. Rock Slope Engineering, fourth ed. Spon Press.
Xinbin, T., Fuchu, D., Xianjing, L., Huiya, Z., 2007. Toppling and stabilization of the intake slope for the Fengtan Hydropower Station enlargement project, Mid-South China. Eng. Geol. 9, 152–167.
Zanbak, C., 1984. Design charts for rock slopes susceptible to toppling. J. Geotech. Eng. 109, 1039–1062.